iScience

CellPress
OPEN ACCESS

Article

Leishmania mexicana centrin knockout parasites promote M1-polarizing metabolic changes

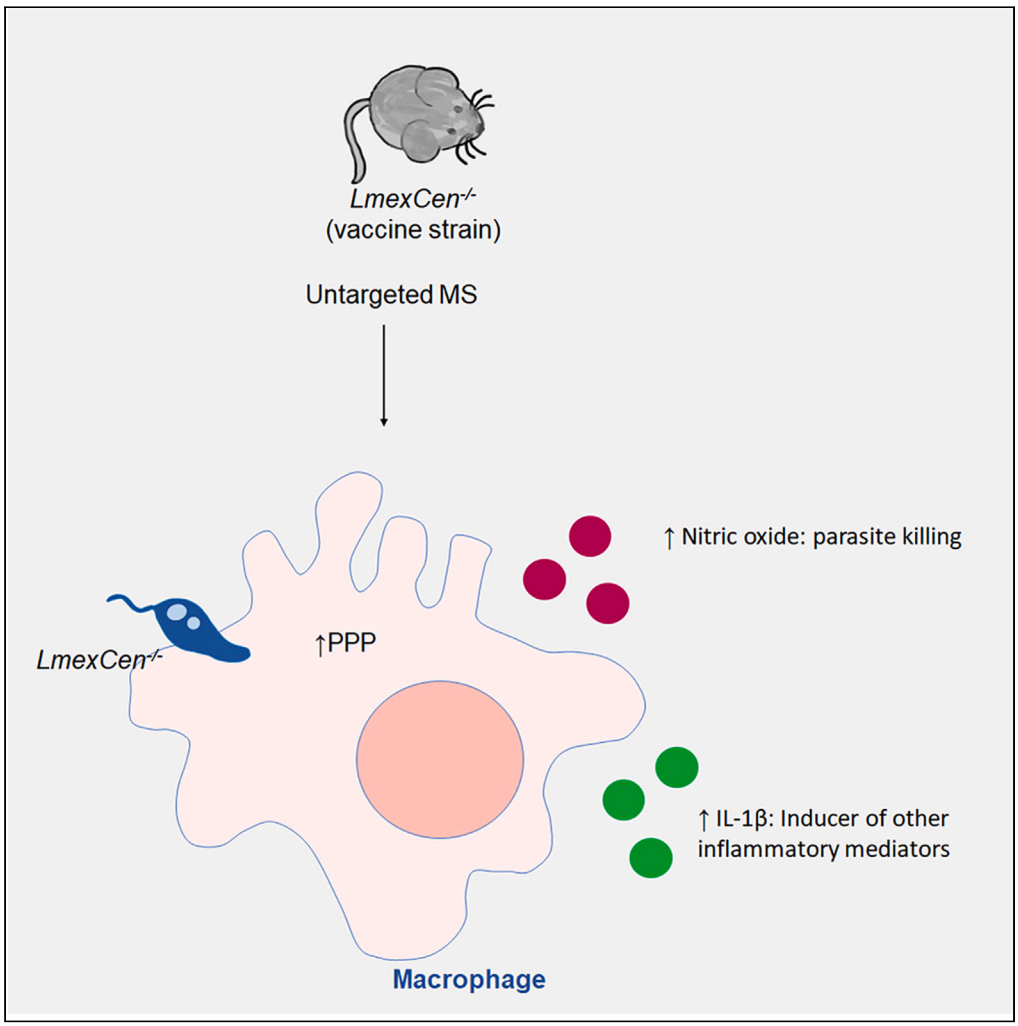

Greta Volpedo, Thalia Pacheco-Fernandez, Timur Oljuskin, ..., Sreenivas Gannavaram, Hira L. Nakhasi, Abhay R. Satoskar

abhay.satoskar@osumc.edu

Highlights

Distinct metabolic regulation occurs in *LmexCen*$^{-/-}$ and *LmexWT* infections

LmexCen$^{-/-}$, but not *LmexWT* infection, induces pentose phosphate pathway (PPP)

Elevated PPP leads to the production of IL-1β and nitric oxide in *LmexCen*$^{-/-}$

PPP enhances the vaccine immunogenicity by polarizing macrophages to M1 phenotype

Volpedo et al., iScience *26*, 107594
September 15, 2023
https://doi.org/10.1016/j.isci.2023.107594

iScience

CellPress
OPEN ACCESS

Article

Leishmania mexicana centrin knockout parasites promote M1-polarizing metabolic changes

Greta Volpedo,[1,2] Thalia Pacheco-Fernandez,[2,3] Timur Oljuskin,[3] Hannah L. Markle,[3] Nazli Azodi,[3] Shinjiro Hamano,[4,5] Greg Matlashewski,[6] Sreenivas Gannavaram,[3] Hira L. Nakhasi,[3] and Abhay R. Satoskar[1,2,7,*]

SUMMARY

Leishmaniasis is a tropical disease prevalent in 90 countries. Presently, there is no approved vaccine for human use. We developed a live attenuated *L. mexicana Cen*$^{-/-}$ (*LmexCen*$^{-/-}$) strain as a vaccine candidate that showed excellent efficacy, characterized by reduced Th2 and enhanced Th1 responses in C57BL/6 and BALB/c mice, respectively, compared to wild-type *L. mexicana* (*Lmex*WT) infection. Toward understanding the immune mechanisms of protection, we applied untargeted mass spectrometric analysis to *LmexCen*$^{-/-}$ and *Lmex*WT infections. Data showed enrichment of the pentose phosphate pathway (PPP) in ears immunized with *LmexCen*$^{-/-}$ versus naive and *Lmex*WT infection. PPP promotes M1 polarization in macrophages, suggesting a switch to a pro-inflammatory phenotype following *LmexCen*$^{-/-}$ inoculation. Accordingly, PPP inhibition in macrophages infected with *LmexCen*$^{-/-}$ reduced the production of nitric oxide and interleukin (IL)-1β, hallmarks of classical activation. Overall, our study revealed the immune regulatory mechanisms that may be critical for the induction of protective immunity.

INTRODUCTION

Leishmaniasis is a protozoan disease with a prevalence of 12 million individuals in more than 90 countries worldwide.[1–3] The most common form is cutaneous leishmaniasis (CL), characterized by skin lesions that can ulcerate and give rise to disfiguring scars, which often attract social stigma.[1,2,4] *Leishmania (L.) mexicana* is the most prevalent causative agent of CL in the New World.[5,6] Despite the elevated morbidity of CL, there are currently no approved human vaccines and the current therapeutic strategies often present significant side effects.[7–9] Our group has previously developed genetically modified *centrin*-deficient *Leishmania* parasites that showed excellent safety and efficacy characteristics in pre-clinical studies.[10,11] *L. major centrin*$^{-/-}$ is now under guanosine monophosphate (GMP) development; however it is unclear whether this Old World strain will be approved as a vaccination strategy or provide cross protection against American *Leishmania* species as *L. major* is not endemic in the New World. For these reasons we have developed *L. mexicana* mutants (*LmexCen*$^{-/-}$) using the CRISPR/Cas9 technique as a candidate vaccine for American leishmaniasis.[12] *LmexCen*$^{-/-}$ amastigote parasites presented a growth defect, which resulted in loss of virulence *in vitro* and *in vivo*. Furthermore, immunization with *LmexCen*$^{-/-}$ did not cause cutaneous lesions in susceptible mouse models and was efficacious against challenge with the virulent strain by eliciting strong protective immunity.[12]

As we continue investigating *LmexCen*$^{-/-}$ parasites as a vaccination strategy, we are interested in understanding the immune determinants of protection and in particular the early drivers of vaccine-mediated immunological profiles. It is well established that *L. mexicana* infection prevents the induction of a pro-inflammatory response by disrupting interferon (IFN)-γ and/or lipopolysaccharide (LPS)-induced nitric oxide (NO) and interleukin (IL)-12 production[13–17] and Th1 differentiation.[18] Furthermore, *L. mexicana* is known to induce expression of arginase and polarize macrophages toward an M2 anti-inflammatory phenotype.[19] On the other hand, *LmexCen*$^{-/-}$ parasites induce protective immunity by diminishing IL-10 and IL-4, potentially produced by M2 macrophages and other regulatory cells.[12] While M2 macrophages are usually associated with susceptibility to CL, M1 macrophages can mediate protection via their antimicrobial functions.[20] Early differentiation into M1 or M2 macrophages can have a profound impact on the development of an effective adaptive immune response; however, the molecular mechanisms by which *LmexCen*$^{-/-}$ parasites lead to classical activation of macrophages have not yet been explored.

A growing body of evidence shows that metabolic changes in macrophages infected with *Leishmania* parasites can impact the availability of nutrients necessary for amastigote replication and affect the cell's polarization and host potential.[21] For instance, M1 macrophages in *Leishmania* dermal granulomas upregulate the pentose phosphate pathway (PPP), important for reactive oxygen species (ROS) production[21] and

[1]Department of Microbiology, The Ohio State University, Columbus, OH 43210, USA
[2]Department of Pathology, Wexner Medical Center, The Ohio State University, Columbus, OH 43210, USA
[3]Division of Emerging and Transfusion Transmitted Diseases, CBER, FDA, Silver Spring, MD, USA
[4]Department of Parasitology, Institute of Tropical Medicine (NEKKEN), The Joint Usage/Research Center on Tropical Disease, Nagasaki University, Nagasaki, Japan
[5]Nagasaki University Graduate School of Biomedical Sciences Doctoral Leadership Program, Nagasaki, Japan
[6]Department of Microbiology and Immunology, McGill University, Montreal, Canada
[7]Lead contact
*Correspondence: abhay.satoskar@osumc.edu
https://doi.org/10.1016/j.isci.2023.107594

M1 effector responses.[22] The PPP has also been shown to control the replication of *Trypanosoma cruzi*, another protozoan parasite, in macrophages by promoting ROS and NO release.[23] Interestingly, upregulation of the PPP in macrophages occurs within 1 h of LPS stimulation and several hours prior to the induction of pro-inflammatory mediators such as superoxide, IL-1β, tumor necrosis factor (TNF)-α, IL-6, and IL-12.[24] These observations highlight the temporal pattern of macrophage activation and suggest that metabolic changes occur prior to, and may cause, immunological changes.

Recent studies have started exploring the role of metabolic changes as drivers of immunomodulation in the context of vaccination. For instance, neutrophils, monocytes, and macrophages undergo metabolic reprogramming following immunization with Bacillus Calmette-Guérin (BCG), a live attenuated vaccine for tuberculosis, which results in a protective immune response.[25,26] In macrophages, this immune response is specifically induced by the activation of aerobic glycolysis.[26] These studies suggest an important role for metabolic reprogramming in vaccination-mediated immunity against pathogens.

Interestingly, studies with other pathogens show that vaccinated individuals display defined metabolic signatures compared to those who did not receive the vaccine, which could be used as reliable biomarkers of protection and vaccine efficacy.[27] Live attenuated vaccines have also been shown to harbor significant metabolic differences compared to their parental strains, as in the case of *Mycobacterium tuberculosis* and the live attenuated *Mycobacterium tuberculosis* vaccine candidate (MTBVAC).[28] Different metabolic profiles in parental and mutant strains could translate into metabolic changes within the host cell depending on exposure to the vaccine or the virulent pathogen. These observations highlight how determining pathogen and strain-specific metabolic reprogramming, as well as their subsequent effects on biological and immunological downstream processes, is a useful tool to identify and characterize unique biomarkers of vaccination.

Toward the goal of uncovering specific metabolic signatures associated with vaccination, our group has sought to explore the immune determinants underlying protection after immunization with *Cen*$^{-/-}$ *Leishmania* mutants. In particular, we previously showed that immunization with *LmexCen*$^{-/-}$ leads to enhanced Th1 responses in C57BL/6 mice.[12] In this study, we aim to investigate some of the metabolic drivers of these immunological changes. We explored the metabolic profiles occurring locally at the inoculation site after immunization with *LmexCen*$^{-/-}$ to understand where some of the immunological responses originate, which we have previously reported. We were also interested in comparing *LmexCen*$^{-/-}$ immunization with wild-type L. mexicana (*LmexWT*) infection to investigate whether there are any differences in the metabolic changes that can explain the divergent immune responses we observe in vaccinated compared to control mice. We chose a 7-day time point to specifically explore the early changes that can shape the immune responses and drive resistance or susceptibility. We found several metabolic pathways enriched in *LmexCen*$^{-/-}$ infected ears and draining lymph nodes that are consistent with the protective immune response observed after immunization. To our knowledge, this is the first report utilizing metabolomics to investigate metabolomic drivers of immune responses in the context of a *Leishmania* vaccine.

RESULTS

Ear tissue of mice immunized with *LmexCen*$^{-/-}$ displays metabolic differences compared to naive mice and mice infected with *Lmex*WT

We collected the ear tissue from mice immunized with *LmexCen*$^{-/-}$, infected with *Lmex*WT, and naive mice and performed untargeted mass spectrometry analysis to identify unique metabolic signatures of disease and vaccination at day seven (Figure 1A). First, we showed no differences in the parasitic burden of ears and draining lymph nodes (dLN) (Figure 1B) that could cause a bias in the metabolic signatures reported herein. Then, using volcano plots, which plot fold change in the x axis and significance in the y axis, we selected significant features from the positive (Figure 1C) and negative (Figure 1D) modes of mass spectrometry analysis. The peaks identified with the positive mode correspond to protonated molecules, while those identified with the negative mode correspond to deprotonated analytes. A fold change threshold (x) 2 and t-tests threshold (y) 0.05 were set for the volcano plots (Figures 1C and 1D). We have then used significant features from the volcano plots for further analysis. We have also used partial least squares-discriminant analysis (PLS-DA), a supervised multivariate analytic approach, to select metabolites from the three comparisons. As shown in Figures 1E and 1F for the positive and negative modes, respectively, naive mice and the groups inoculated with either *LmexCen*$^{-/-}$ or *Lmex*WT each displayed unique metabolic signatures, highlighting a significant *Leishmania*-specific metabolic shift with distinct characteristics depending on whether the mice were exposed to the mutant or parental strain.

Immunization with *LmexCen*$^{-/-}$ leads to M1-polarizing metabolic changes at the inoculation site

In order to identify specific metabolic pathways enriched in mice immunized with *LmexCen*$^{-/-}$, we used both mummichog and gene set enrichment analysis (GSEA). Mummichog analysis uses an algorithm that predicts functional activity bypassing metabolite identification, while GSEA requires the metabolites to be identified before pathway/network analysis. We used the Integrated MS Peaks to Pathways plot to summarize the results of the Fisher's method for combining mummichog (y) and GSEA (x) p values from the positive (Figure 2A) and negative (Figure 2B) mode datasets, indicating the metabolic pathways enriched in the ear tissue of different groups. We were interested in identifying any significantly enriched pathways known to promote a pro-inflammatory protective immune response in immunized mice compared to naive controls. We identified aspartate metabolism and PPP, which are involved in M1 polarization of macrophages to be enriched in *LmexCen*$^{-/-}$ immunization.[21,24,29] Our results showed enriched alanine, aspartate, and glutamate metabolism in the ears of *LmexCen*$^{-/-}$ immunized mice, compared to naive mice as highlighted by the black box in Figure 2A. Furthermore, the PPP was also enriched in the ears of *LmexCen*$^{-/-}$ immunized mice, compared to naive and *Lmex*WT-infected mice (Figures 2A and 2B). Based on the t scores for the matched metabolites, both aspartate metabolism and the PPP were upregulated in the *LmexCen*$^{-/-}$ immunized group,

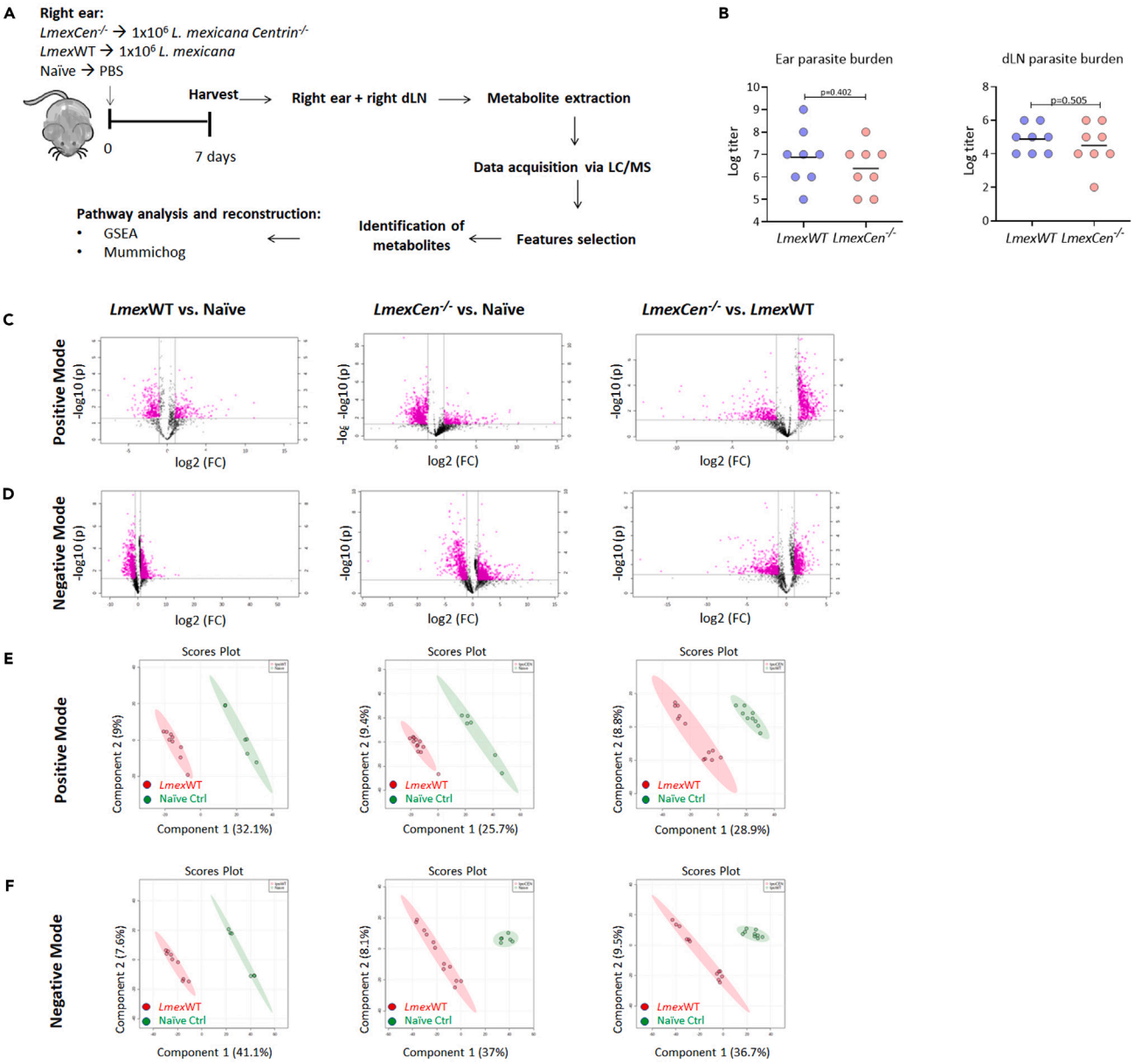

Figure 1. Infection with *Lmex*WT and immunization with *LmexCen*$^{-/-}$ display different metabolic signatures in at the inoculation site

(A) Experimental design for metabolomic analysis of infection with *Lmex*WT and immunization with *LmexCen*$^{-/-}$. Female C57BL/6 mice were injected intradermally in the ear with stationary phase *Lmex*WT, *LmexCen*$^{-/-}$ parasites, or PBS. After 7 days, the injected ears and their respective draining lymph nodes (dLN) were collected and processed for mass spectrometry. The data acquired was used to identify enriched metabolites and determine activated pathways in the tissue. N = 5 for each group.

(B) At day 7, parasite burden in the ear and dLN was determined using limiting dilutions. Data are represented as scattered dot plots with line at mean, p values are shown among groups. N = 8 for each group.

(C and D) (C) Normalized data from ear tissue from C57BL/6 mice after 7 days of infection with *Lmex*WT, immunization with *LmexCen*$^{-/-}$, or naive control was used to perform statistical analysis. C, D) Features selected by volcano plot from positive (C) and negative (D) modes for ear tissue of *Lmex*WT vs. naive, *LmexCen*$^{-/-}$ vs. naive, and *LmexCen*$^{-/-}$ vs. *Lmex*WT mice using LC/MS with fold change threshold (x) 2 and t-tests threshold (y) 0.05. Both fold changes and p values are log transformed.

(E and F) Partial least squares-discriminant analysis (PLS-DA) from positive (E) and negative (F) mode for ear tissue of *Lmex*WT vs. naive, *LmexCen*$^{-/-}$ vs. naive, and *LmexCen*$^{-/-}$ vs. *Lmex*WT mice. Abbreviations: LC/MS: liquid chromatography/mass spectrometry; GSEA: gene set enrichment analysis.

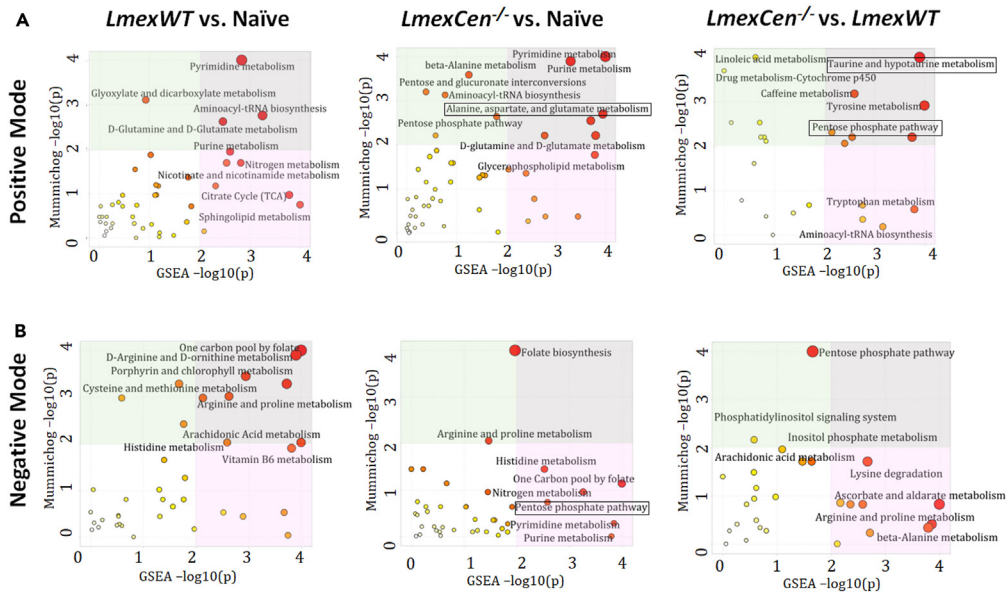

Figure 2. Metabolic pathways enriched in mice infected with *Lmex*WT or immunized with *LmexCen*$^{-/-}$ at the inoculation site

(A and B) Normalized data from ear tissue from C57BL/6 mice after 7 days of infection with *Lmex*WT, immunization with *LmexCen*−/−, or naive control was used to perform peaks to pathway analysis. Using the MS Peaks to Paths module in MetaboAnalyst5.0, the mummichog and gene set enrichment analysis (GSEA) p values were combined. The Integrated MS Peaks to Paths plot summarizes the results of the Fisher's method for combining mummichog (y) and GSEA (x) p values from the positive (A) negative (B) mode datasets, indicating the metabolic pathways enriched. The size and color of the circles correspond to their transformed combined p values. Large and red circles are considered the most perturbed pathways. The colored areas show the significant pathways based on either mummichog (blue) or GSEA (pink), and the purple area highlights significant pathways identified by both algorithms. Highlighted by the black boxes are pathways associated with a protective immune response against leishmaniasis.

revealing a mechanism for protection mediated by *LmexCen*$^{-/-}$ parasites. The metabolites D-erythrose 4-phosphate, sn-glycerol 3-phosphate, 3-ketolactose, D-glucose, melibiose, and thiamin diphosphate were significantly upregulated in the *LmexCen*$^{-/-}$ inoculated group, as identified using Metscape[30] (Figure 3). Table 1 shows all PPP mediators enriched in the *LmexCen*$^{-/-}$ dataset compared to the naive dataset.

Co-culture with *LmexCen*$^{-/-}$ parasites leads to PPP-dependent M1 phenotype in macrophages

Our mass spectrometry analysis revealed upregulated PPP in the *LmexCen*$^{-/-}$ group, which is known to polarize macrophages toward an M1 phenotype.[31] We have previously observed enhanced pro-inflammatory responses following *LmexCen*$^{-/-}$ immunization *in vitro* and *in vivo*;[12] however it is not yet known whether the PPP significantly contributes to driving this immune profile. In order to investigate this, we measured NO, IL-1β, and IL-12 in bone marrow-derived macrophages (BMDMs) cultured with *LmexCen*$^{-/-}$ or *Lmex*WT parasites and stimulated with LPS in presence or absence of the PPP inhibitors 6-aminonicotinamide (6-AN) and dehydroepiandrosterone (DHEA) (Figure 4A). NO, IL-1β, and IL-12 are hallmark mediators of M1 macrophages induced by the PPP and involved in parasite killing and the induction of Th1 immune responses.[20,22,32,33] Our results showed that infection with *LmexWT* or *LmexCen*$^{-/-}$ parasites induced NO production in BMDMs in the presence of LPS. The level of NO observed in infected macrophages was higher than that in cells treated with LPS alone, showing that the effect is due to the infection rather than to the stimulation with LPS (Figure 4B). *LmexCen*$^{-/-}$ infected BMDMs produced more NO compared to *LmexWT*-infected cells (Figure 4B). Treatment with 6-AN, a competitive inhibitor of nicotinamide adenine dinucleotide phosphate (NADP+)-dependent enzyme glucose-6-phosphate dehydrogenase (G6PD),[34] resulted in a significant reduction in NO production of macrophages infected with *LmexWT*, but not *LmexCen*$^{-/-}$, compared to their respective untreated controls. On the other hand, treatment with DHEA, a non-competitive inhibitor of G6PD,[35] also reduced NO levels *in vitro* in BMDMs infected with *LmexCen*$^{-/-}$ mutants, but not *LmexWT*, compared to their respective untreated controls (Figure 4B), suggesting that inhibition of the PPP causes impaired NO production. Treatment with DHEA, but not with 6-AN, showed a statistically significant reduction in the production of IL-1β in BMDMs infected with either *LmexWT* or *LmexCen*$^{-/-}$ (Figure 4C). *L. mexicana* infection is known to inhibit LPS and IFN-γ-induced IL-12 production in macrophages.[14,16,36,37] Consistent with these results, both *LmexWT* and *LmexCen*$^{-/-}$ infections diminished the LPS-induced IL-12 production compared to no infection control (Figure 4D). Treatment with 6-AN and DHEA showed a reduction of IL-12 in *LmexWT* and *LmexCen*$^{-/-}$-infected BMDMs compared to the LPS-alone control and the respective untreated infection controls (Figure 4D). Taken together, these results highlight a role for PPP in *LmexCen*$^{-/-}$-mediated M1 polarization and pro-inflammatory effector functions in macrophages (Figure 5).

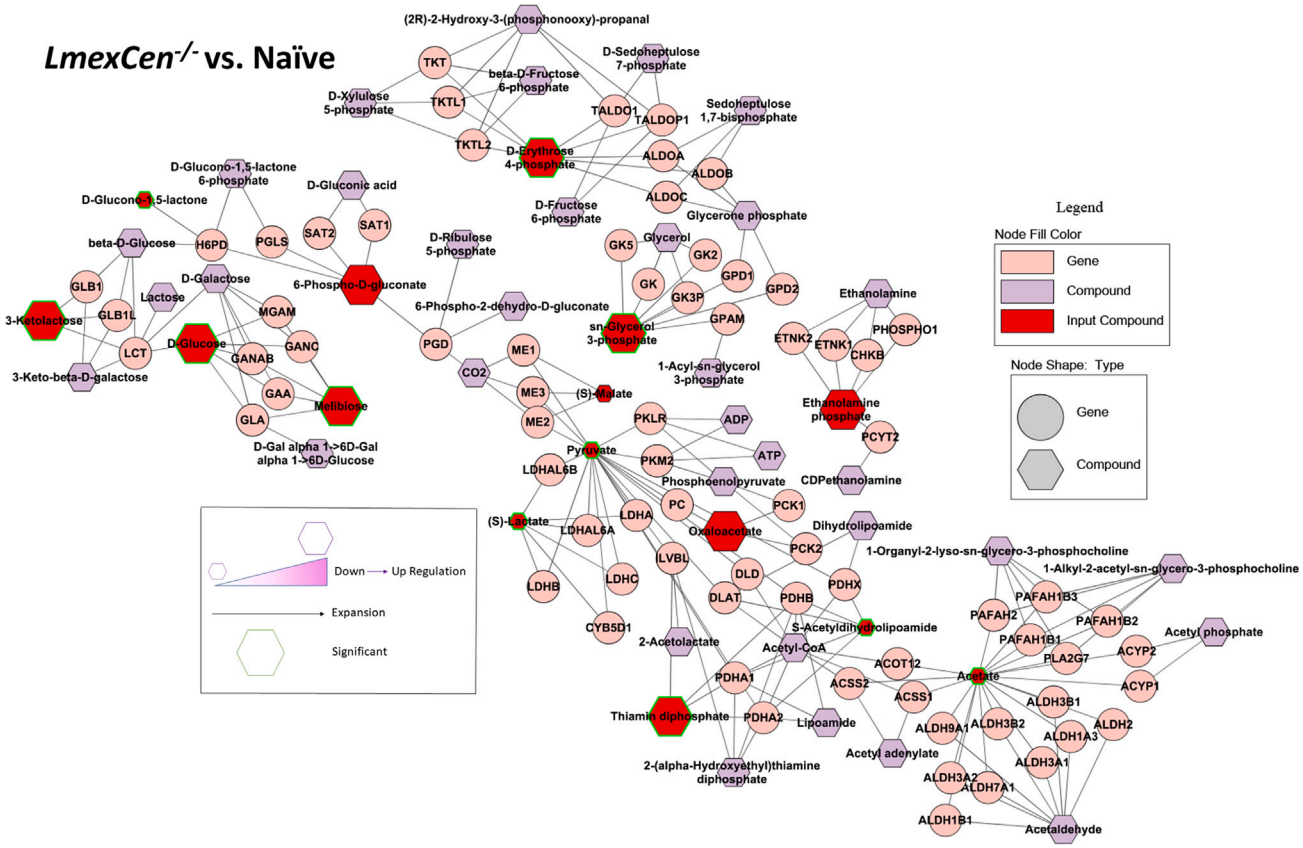

Figure 3. Immunization with *LmexCen*$^{-/-}$ leads to enriched pentose phosphate pathway metabolism

Normalized data from ear tissue from C57BL/6 mice after 7 days of immunization with *LmexCen*$^{-/-}$ and naive control was used to perform statistical analysis. Metabolite network identified with Metscape. Metabolites of the Pentose Phosphate Pathway are represented in this graph. Larger hexagons represent upregulation, while smaller hexagons represent down-regulation. Red hexagons represent compounds detected in the dataset, while hexagons with a green outline represent statistically significant metabolites (p value $\leq$0.05). The purple hexagons represent compounds that are associated with the pathway but are not detected in the input dataset. The pink circles represent the genes regulating the biosynthetic activities.

Leishmania-centrin deficiency results in differential host metabolic reprogramming, compared to *LmexWT* infection

After identifying metabolic drivers of immune protection in immunized compared to non-immunized models, we explored the host metabolic differences mediated by *LmexCen*$^{-/-}$, compared to *Lmex*WT parasites. Interestingly, the arginase, alanine, aspartate, and glutamate metabolism, the taurine and hypotaurine metabolism, as well as PPP, identified in the ears of immunized mice were not enriched in the *Lmex*WT-infected group compared to naive mice (Figures 2A and 2B), highlighting differential metabolic regulation following exposure to the mutant or parental strain of *L. mexicana*. Table 1 shows all PPP mediators enriched in the *LmexCen*$^{-/-}$ dataset compared to the *Lmex*WT dataset.

Our combined mummichog and GSEA analysis also revealed the enrichment of taurine and hypotaurine metabolism in ears immunized with *LmexCen*$^{-/-}$, compared to those infected with *Lmex*WT parasites (Figure 2A). This pathway is known to play a role in the healing of CL lesions,[38] and it was upregulated in the *LmexCen*$^{-/-}$ group, based on the t scores of the matched metabolites. In particular, the taurine/hypotaurine metabolite glutaurine was altered in *LmexCen*$^{-/-}$-immunized mice, compared to *Lmex*WT-infected mice.

A Venn diagram of the metabolic pathways enriched in the ears of mice infected with *Lmex*WT or immunized with *LmexCen*$^{-/-}$, compared to uninfected naive mice is shown in Figure 6. Despite a handful of common pathways, the majority of metabolic changes seem to be strain specific, suggesting that *centrin* deletion leads to divergent metabolic regulation of the mammalian host cell.

Taken together, our results show that *LmexCen*$^{-/-}$ parasites lead to differential metabolic reprogramming, compared to the WT strain. In particular, the *LmexCen*$^{-/-}$ mutants promote metabolic profiles known to drive protective immunity against leishmaniasis.

Draining lymph nodes display different metabolic reprogramming, compared to cutaneous tissue during early exposure to *Leishmania*

After exploring metabolic reprogramming locally at the inoculation site, we were interested in investigating metabolic changes in the draining lymph nodes in the early stages of the infection. Similarly, to the process we used for the ear tissue, volcano plots were employed to select significant features from the positive (see Figure S1A) and negative (see Figure S1B) modes and PLS-DA to identify variations among the

Table 1. Pentose phosphate pathway mediators enriched in the *LmexCen*$^{-/-}$ and *Lmex*WT datasets

Dataset	Compound Name	HMDB ID	p value	Log FC
LmexCen$^{-/-}$ vs. Naive	D-Gluconolactone	HMDB0000150	0.07614	0.469463
		HMDB0000150	0.00323	Infinity
		HMDB0000150	0.06476	0.438271
		HMDB0000150	0.03838	−0.83846
	2-deoxy-D-ribose-5-phosphate	HMDB0001031	0.05156	0.430808
	Fructose-6-phosphate	HMDB0000124	0.01374	0.859422
		HMDB0000124	0.013	0.374674
		HMDB0000124	0.11882	Infinity
		HMDB0000124	0.04761	0.097545
LmexWT vs. *LmexCen*$^{-/-}$	D-Gluconolactone	HMDB0000150	0.37318	−0.16859
		HMDB0000150	0.02529	−0.21483
	2-deoxy-D-ribose-5-phosphate	HMDB0001031	0.24624	−0.19461
	Fructose-6-phosphate	HMDB0000124	0.00016	−0.22084
		HMDB0000124	0.00478	−0.70155
		HMDB0000124	0.00537	−0.57994
		HMDB0000124	0.15585	−0.65417
		HMDB0000124	0.08191	0.145185
		HMDB0000124	0.01194	−0.75432
		HMDB0000124	0.27226	−0.22221
		HMDB0000124	0.14201	−0.74394
LmexWT vs. Naive	D-Gluconolactone	HMDB0000150	0.0207	Infinity
		HMDB0000150	0.04355	0.315925
	Fructose-6-phosphate	HMDB0000124	0.00375	0.211366
		HMDB0000124	0.0097	0.408554
		HMDB0000124	0.01975	−0.54961
		HMDB0000124	0.02603	−0.1233
		HMDB0000124	0.55928	0.180685

Normalized data ear tissue from C57BL/6 mice inoculated with *LmexCen*$^{-/-}$, *Lmex*WT or naïve controls was used to identify pentose phosphate pathway metabolites. HMDB, Human metabolome database.

experimental groups from the positive (see Figure S1C) and negative (see Figure S1D) modes. Overall, our results show distinct metabolic signatures in the draining lymph nodes of mice inoculated with either *LmexCen*$^{-/-}$ or *Lmex*WT, and naive controls, in a manner comparable to what we observed locally in the ear skin tissue.

Interestingly, mass spectrometry analysis of lymph node tissue revealed different results from what we found locally in the ears. While we did not observe enrichment of the same M1-promoting pathways in *LmexCen*$^{-/-}$-immunized mice, our data show enriched linoleic acid metabolism in the group immunized with *LmexCen*$^{-/-}$ mutants, compared to naive mice (see Figures S2A and S2B). Based on the t scores for the matched metabolites, this pathway was activated in the *LmexCen*$^{-/-}$-group. This pathway has previously been shown to promote a protective immune response in visceral *leishmaniasis* and could provide a mechanism of protection in the lymph nodes.[39] We also found several other pathways that were uniquely or consistently enriched in the draining lymph nodes of *LmexCen*$^{-/-}$-immunized and *Lmex*WT-infected mice, compared to the naive group (see Figure S3). Despite the presence of a few common pathways, the majority of metabolic changes seem to be strain specific, similarly to what we previously observed in the ears.

DISCUSSION

American CL is a disfiguring disease that lacks effective preventive strategies. We have recently developed a live attenuated *L. mexicana* parasite lacking the *centrin* gene (*LmexCen*$^{-/-}$) that showed excellent safety and efficacy characteristics in pre-clinical models.[12] Immunization with *LmexCen*$^{-/-}$ parasites resulted in alteration of Th1/Th2 responses in C57BL/6 mice. In this study, we investigated the metabolic drivers of these immunological profiles.

Although a lot of attention has been given to the role of chemokines and cytokines in *Leishmania* infection, other factors may also influence the immunity against CL. Factors such as microRNAs,[40,41] epigenetic reprogramming, and metabolic mediators[20] have more recently been

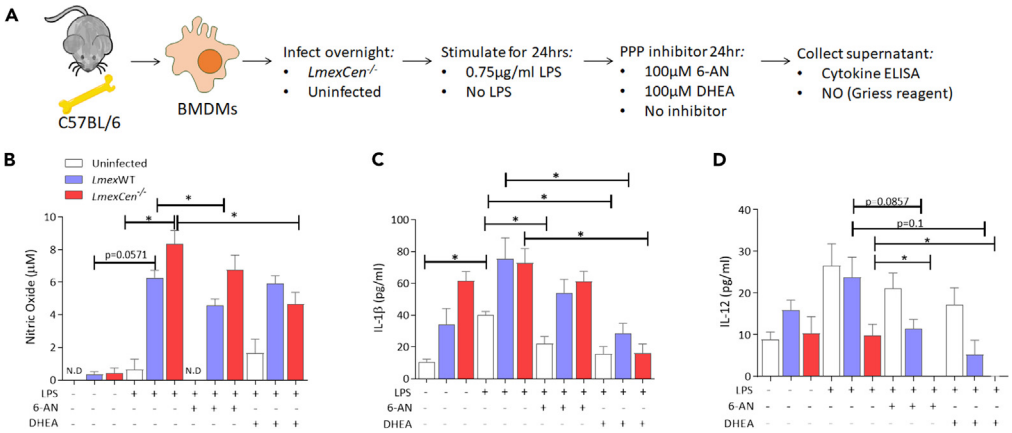

Figure 4. Pentose phosphate pathway-dependent nitric oxide, IL-12, and IL-1β release in BMDMs

(A) BMDMs were extracted from C57BL/6 mice and cultured with medium or *LmexCen*$^{-/-}$ and stimulated *in vitro* by LPS for 24 h, and 6-AN or DHEA for 24 h. (B–D) (B) Nitric oxide production was determined by Griess reaction. (C) IL-1β and (D) IL-12 production were determined by cytokine ELISA. Data are represented as mean ± SEM. Data represents one of three experiments with N = 3–5 per group. *p < 0.05, unpaired *t* test. Abbreviations: LPS, lipopolysaccharide; 6-AN, 6-aminonicotinamide; DHEA, dehydroepiandrosterone; NO, nitric oxide.

investigated. Specifically, metabolomics is emerging as a useful tool to uncover previously unknown signaling networks that govern immune regulation and confer functional specialization. Such metabolic remodeling of immune cell activity has not been extensively explored in vaccine immunity.

We have previously observed critical differences in the immunological responses following inoculation with *LmexCen*$^{-/-}$ parasites compared to their wild-type (WT) counterparts.[12] This was also observed in *L. donovani*, *L. major*, and *L. mexicana* centrin mutants.[10,12,42,43] Immunization with *LmCen*$^{-/-}$ and *LmexCen*$^{-/-}$ has been shown to confer protection against homologous and heterologous challenges.[10–13,44] However, the immune mechanisms of protection differed in these two immunization regimens. The protective immunity induced by *LmCen*$^{-/-}$ was mediated by an elevated Th1 response characterized by IFN-γ-, TNF-α-, and IL-2-producing T cells expressing the clusters of differentiation (CD) CD4$^+$ and CD8$^+$, whereas in *LmexCen*$^{-/-}$ immunization, protection was mediated mainly by a reduction of IL-10/IL-4 by the CD4$^+$ and CD8$^+$ T cells in C57BL/6 mice and an elevated Th1 response characterized by IL-12 and IFN-γ in BALB/c mice.[12] In this study, we explored the metabolic drivers of the immunological differences between infection with the parental or mutant strains and demonstrated that immunization with *LmexCen*$^{-/-}$ parasites results in unique metabolic changes, compared to naive and *Lmex*WT-infected mice.

One of the metabolic pathways enriched in the ears of *LmexCen*$^{-/-}$ immunized mice, compared to naive mice, was aspartate metabolism, which is known to induce M1 polarization in macrophages, as well as the production of IL-1β and TNF-α. Consistent with these findings, we observed activated PPP metabolism in the ears of *LmexCen*$^{-/-}$ immunized mice, compared to naive mice, and to mice infected with *Lmex*WT. It is well established that M1 macrophages upregulate glycolysis and PPP in order to generate ATP and nicotinamide adenine dinucleotide phosphate hydrogen (NADPH), utilized for the production of ROS and reactive nitrogen species (RNS).[21,24] Pro-inflammatory M1 macrophages are crucial for mounting a protective immune response against CL, as they release ROS and RNS (such as NO) to kill the parasites, and act as antigen-presenting cells to prime T cells in order to polarize them toward a Th1 phenotype.[20,45,46] The upregulation of aspartate metabolism and PPP at the inoculation site suggests a switch to a protective pro-inflammatory phenotype in macrophages following *LmexCen*$^{-/-}$ inoculation. These results are consistent with previous literature showing that an induction in PPP can control the replication of the protozoan parasite *Trypanosoma cruzi* via NO-mediated killing.[23] Our results show an increase in NO and IL-1β production by BMDMs cultured with either *LmexWT* or *LmexCen*$^{-/-}$ parasites, in the presence of LPS. LPS is known to increase the PPP flux in macrophages by negating the activity of carbohydrate kinase-like protein (CARKL).[31] In our data NO and IL-β concentrations were higher in both infection groups compared to LPS treatment, showing that the observed effects are infection induced rather than an effect of LPS. NO and IL-1β have been reported as products of M1 macrophages with enhanced PPP and glycolysis.[31] PPP activation results in the generation of NADPH, a co-factor of inducible nitric oxide synthase (iNOS), the enzyme responsible for the production of NO.[31] Pyruvate, a product of glycolysis downstream of PPP, enters the tricarboxylic acid cycle (TCA) cycle after conversion into Acetyl-CoA. However, M1 macrophages are associated with a truncated TCA cycle that results in an accumulation of succinate which stabilizes the transcription factor hypoxia-inducible factor 1-alpha (HIF-1α) that induces the transcription of IL-1β.[31,47] Our data showed that both NO and IL-1β concentrations are reduced after inhibition of PPP using two different G6PD inhibitors, which demonstrates a role for PPP in *LmexCen*$^{-/-}$-mediated M1 polarization and pro-inflammatory effector functions in macrophages.

The use of two different PPP inhibitors allowed us to confirm the involvement of this pathway in *LmexCen*$^{-/-}$ infection. Both inhibitors target the enzyme G6PD and therefore inhibit NADPH production. Of the two, 6-AN is a competitive inhibitor, while DHEA is a non-competitive inhibitor of G6PD.[48] Testing with both 6-AN and DHEA in our experiments is relevant since multiple studies comparing the effect of these inhibitors in various diseases models suggested that the effect of DHEA and 6-AN is different and the duration of their effects is not the

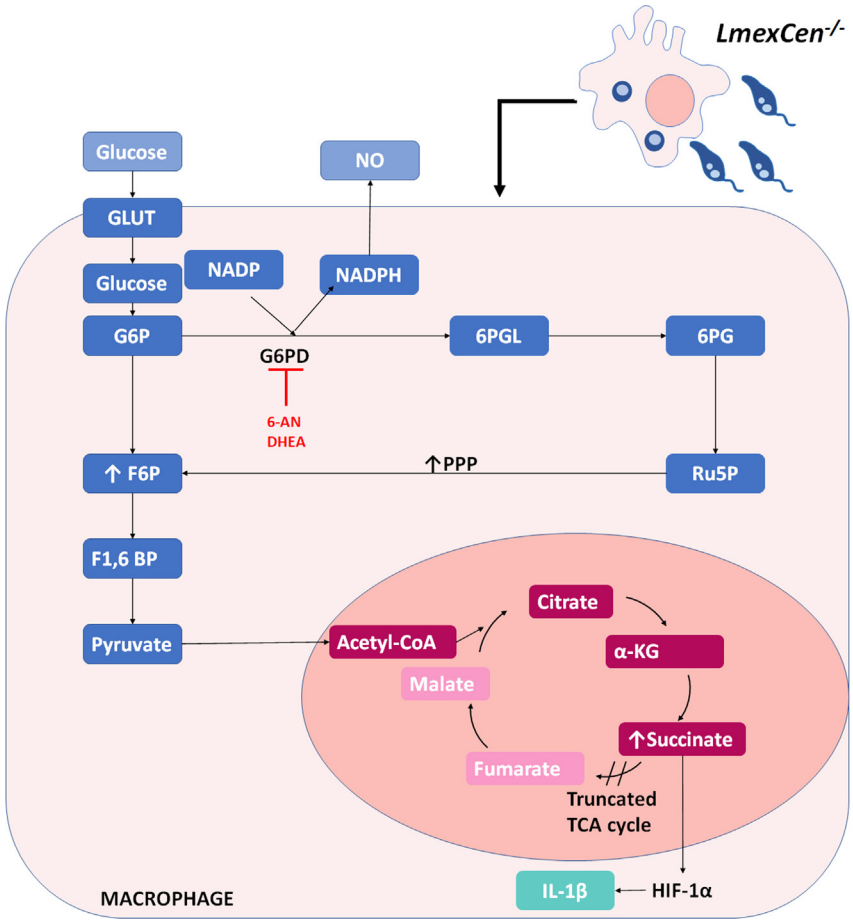

Figure 5. Immunization with *LmexCen*$^{-/-}$ parasites leads to induction of pentose phosphate pathway

Graphical scheme showing that during *LmexCen*$^{-/-}$-immunization, BMDMs differentiate into M1. The activation of the PPP results on the generation of NADPH trough the enzyme G6PD, target of 6-AN and DHEA inhibitors. NADPH is a co-factor of iNOS therefore this pathway leads to the production of NO. On the other hand, the activation of the tricarboxylic acid cycle (TCA), truncated in M1 macrophages, leads to the accumulation of succinate in the cell, which then stabilized HIF-1α resulting in the transcription of IL-1β. Abbreviations: GLUT, glucose transporter; G6P, glucose 6-phosphate; F6P, fructose 6-phosphate; F1,6BP, fructose-1,6-bisphosphate; G6PD, glucose-6-phosphate dehydrogenase; 6PGL, 6-phosphogluconolactone; 6PG, 6-phosphogluconate; RU5P, ribulose-5-phosphate; NADPH, Nicotinamide adenine dinucleotide phosphate; NO, nitric oxide, Alpha-Ketoglutarate, HIF-1α; Hypoxia-inducible factor 1-alpha.

same.[48–50] Specifically, studies on T cells metabolic reprograming, where the treatment with DHEA and 6-AN was carried out to inhibit PPP, showed differential effects on IFN-γ production.[50] Consistently, we observed differential inhibition in the LPS-induced NO production after infection with *Lmex*WT and *LmexCen*$^{-/-}$ using both PPP inhibitors confirming our hypothesis that PPP is importantly involved in the M1 phenotype of *LmexCen*$^{-/-}$ infected macrophages.

In our *in vitro* experiments we observed that the LPS-induced IL-12 levels decreased following infection of BMDMs from the resistant C57BL/6 mice with either *LmexWT* or *LmexCen*$^{-/-}$ parasites. This result is in agreement with previous reports which showed that LPS-induced IL-12 production is dampened in *L. mexicana* infection due to parasite-induced nuclear factor κB (NF-κB) degradation.[14,16,36,37] Interestingly, we have previously observed that infection of BMDMs from the susceptible BALB/c mice with *LmexCen*$^{-/-}$ parasites resulted in an elevated IL-12 production, above the level observed in LPS treatment[12] suggesting that host genetic background influences the macrophage responses to *LmexCen*$^{-/-}$ infection.

These observations are particularly interesting since *L. mexicana* WT parasites are known to polarize macrophages toward an M2 anti-inflammatory phenotype.[19] This is consistent with previous results showing that *L. donovani Cen*$^{-/-}$ parasites also promote an M1 phenotype in macrophages, in contrast to *L. donovani* WT infection.[51]

In addition to its role in NO and IL-1β production in macrophages, PPP has also been shown to be critical for neutrophil extracellular traps (NETs) formation (NETosis) that requires superoxide production through NADPH oxidase activity in neutrophils.[52] Elevated PPP observed in *LmexCen*$^{-/-}$ infection could have similar roles in neutrophils, thought that needs to be experimentally demonstrated. Further studies are warranted to determine which other cell types predominantly and consistently upregulate aspartate metabolism, as well as the PPP, at the site of inoculation after exposure to *LmexCen*$^{-/-}$ mutants. In particular, it would be interesting to determine whether the PPP remains

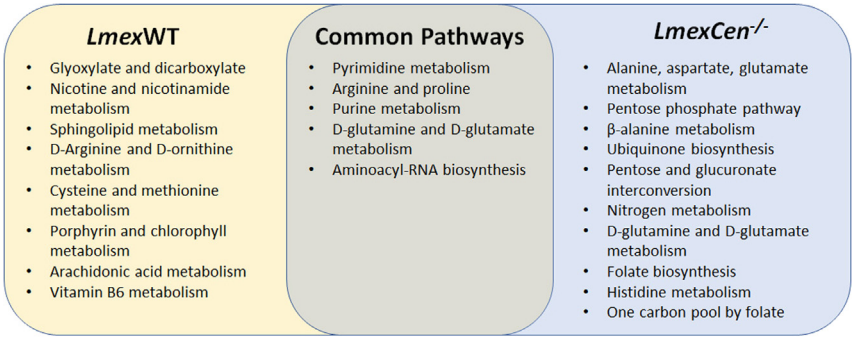

Figure 6. Unique and common pathways enriched in the ears following *LmexCen*−/− immunization or *Lmex*WT infection

Venn diagram of the metabolic pathways significantly enriched based on mummichog and GSEA analysis in the ear of C57BL/6 mice after 7 days of infection with *Lmex*WT or immunization with *LmexCen*−/−, compared to uninfected naive mice.

enriched during the adaptive immune response as this pathway has been shown to be upregulated in activated and proliferating T cells[53] and it is the signature metabolic pathway of effector T cells.[54]

Our analysis also revealed activated taurine and hypotaurine metabolism in the ears of *LmexCen*$^{-/-}$ immunized mice, compared to mice infected with *Lmex*WT. Taurine is known to have anti-apoptotic, antioxidant, and cytoprotective functions,[55] and it promotes wound healing in CL lesions caused by *L. major*.[38] Furthermore, taurine induces the expression of type I IFN-signature genes and promotes phosphorylation of IFN regulatory factor (IRF)-7 in dendritic cells (DCs).[56] IRF-7 is crucial for macrophage killing of *L. donovani* in the liver and spleen, and the lack of this factor leads to impaired CD4^{+} T, natural killer (NK), and natural killet T cells (NKT) activity in the liver.[57,58] Additional studies are required to determine the phosphorylation state of IRF-7 and the subsequent immunoregulation following exposure with *LmexCen*$^{-/-}$ or *Lmex*WT parasites.

In this study we also analyzed metabolic changes in the draining lymph nodes. Interestingly, the metabolic signatures in the draining lymph nodes at 7 days post-infection were somewhat different compared to what we observed at the lesion site. Nevertheless, we found enrichment of linoleic acid (LA) metabolism in *LmexCen*$^{-/-}$ immunized mice, compared to mice infected with *Lmex*WT. It has been recently shown that LA inhibits *L. donovani* survival in macrophages and promotes production of superoxide by neutrophils and macrophages.[39] Furthermore, LA is a precursor of ω-6 polyunsaturated fatty acids (PUFAs), and deficiency of PUFAs impairs cell-to-cell interaction, resulting in improper antigen presentation and inadequate lymphocyte activation.[39] Thus, the intake of appropriate amounts of LA through diet can make a difference between resistance and susceptibility to *L. donovani* in patients.[39] Although these results have not been validated in other species of *Leishmania*, they may affect mechanisms of vaccine immunity.

Expectedly, metabolomics analysis indicated several pathways were enriched consistently or uniquely among immunized and infected mice, as illustrated in the Venn diagrams. In this study we focused on the PPP, as well as aspartate, taurine, and linoleic acid metabolism, due to their known immunomodulatory functions. In particular, *LmexCen*$^{-/-}$-mediated activation of the PPP leads to the upregulation of pro-inflammatory cytokines in macrophages, indicative of an M1 phenotype. Pro-inflammatory antigen-presenting cells play a crucial role in inducing a Th1 adaptive response, which has been previously shown to promote *LmexCen*$^{-/-}$-mediated protection against CL.[12] An analogous analysis of *LmCen*$^{-/-}$ infected ear tissue at the identical time point following immunization revealed that tryptophan metabolism is significantly altered between *LmCen*$^{-/-}$ and *LmWT* infections, while PPP remained unaltered, suggesting that similarly attenuated parasite strains utilize distinct metabolic immunoregulatory circuits.[59]

In conclusion, uncovering the unique metabolic signatures of vaccination and disease will be invaluable to reveal immune mechanisms of protection and to identify novel markers of vaccine efficacy against leishmaniasis.

Limitations of the study

The results in Table 1 show one of the complications of untargeted metabolomics, which is the presence of multiple isoforms of the same compound that can sometimes have opposite fold change directions and create potential ambiguity in the interpretation of the results. Additionally, the annotation of the metabolites (shown with HMDB identifiers) is tentative as they are based exclusively on the formula with no additional information regarding the compound structures.

STAR★METHODS

Detailed methods are provided in the online version of this paper and include the following:

- KEY RESOURCES TABLE
- RESOURCE AVAILABILITY
  - Lead contact

SUPPLEMENTAL INFORMATION

Supplemental information can be found online at https://doi.org/10.1016/j.isci.2023.107594.

ACKNOWLEDGMENTS

This study was funded by Global Health Innovative Technology Fund to A.R.S. and S.H. (GHIT 2020-0134). The authors thank the Campus Chemical Instrument Center (CCIC) Mass Spectrometry and Proteomics Facility at The Ohio State University (OSU) for their help.

Our contributions are an informal communication and represent our own best judgment. These comments do not bind or obligate FDA.

AUTHOR CONTRIBUTIONS

G.V., S.G., H.L.N., and A.R.S. designed the experiments. G.V., T.P.F., and H.L.M. performed the experiments. T.O. and N.A. analyzed the mass spectrometry data. G.V. and S.G. wrote the manuscript. G.V., T.P.F., T.O., N.A., S.G, H.L.N, S.H., G.M., and A.R.S. revised the manuscript.

DECLARATION OF INTERESTS

The FDA is currently a co-owner of two US patents that claim attenuated *Leishmania* species with the *centrin* gene deletion (US7,887,812 and US 8,877,213). This article reflects the views of the authors and should not be construed to represent FDA's views or policies.

Received: September 14, 2022
Revised: June 7, 2023
Accepted: August 7, 2023
Published: August 29, 2023

REFERENCES

1. World Health Organization (2018). Leishmaniasis. http://www.who.int/leishmaniasis/en/.
2. Center for Disease Control and Prevention (2013). Leishmaniasis. https://www.cdc.gov/parasites/leishmaniasis/.
3. McGwire, B.S., and Satoskar, A.R. (2014). Leishmaniasis: clinical syndromes and treatment. QJM *107*, 7–14. https://doi.org/10.1093/qjmed/hct116.
4. Okwor, I., and Uzonna, J. (2016). Social and Economic Burden of Human Leishmaniasis. Am. J. Trop. Med. Hyg. *94*, 489–493. https://doi.org/10.4269/ajtmh.15-0408.
5. Pace, D. (2014). Leishmaniasis. J. Infect. *69*, S10–S18. https://doi.org/10.1016/j.jinf.2014.07.016.
6. Kevric, I., Cappel, M.A., and Keeling, J.H. (2015). New World and Old World Leishmania Infections: A Practical Review. Dermatol. Clin. *33*, 579–593. https://doi.org/10.1016/j.det.2015.03.018.
7. Wolf Nassif, P., DE Mello, T.F.P., Navasconi, T.R., Mota, C.A., Demarchi, I.G., Aristides, S.M.A., Lonardoni, M.V.C., Teixeira, J.J.V., and Silveira, T.G.V. (2017). Safety and efficacy of current alternatives in the topical treatment of cutaneous leishmaniasis: a systematic review. Parasitology *144*, 995–1004. https://doi.org/10.1017/S0031182017000385.
8. Singh, N., Kumar, M., and Singh, R.K. (2012). Leishmaniasis: current status of available drugs and new potential drug targets. Asian Pac. J. Trop. Med. *5*, 485–497. https://doi.org/10.1016/S1995-7645(12)60084-4.
9. de Menezes, J.P.B., Guedes, C.E.S., Petersen, A.L.d.O.A., Fraga, D.B.M., and Veras, P.S.T. (2015). Advances in Development of New Treatment for Leishmaniasis. BioMed Res. Int. *2015*, 815023. https://doi.org/10.1155/2015/815023.
10. Zhang, W.W., Karmakar, S., Gannavaram, S., Dey, R., Lypaczewski, P., Ismail, N., Siddiqui, A., Simonyan, V., Oliveira, F., Coutinho-Abreu, I.V., et al. (2020). A second generation leishmanization vaccine with a markerless attenuated Leishmania major strain using CRISPR gene editing. Nat. Commun. *11*, 3461. https://doi.org/10.1038/s41467-020-17154-z.
11. Karmakar, S., Ismail, N., Oliveira, F., Oristian, J., Zhang, W.W., Kaviraj, S., Singh, K.P., Mondal, A., Das, S., Pandey, K., et al. (2021). Preclinical validation of a live attenuated dermotropic Leishmania vaccine against vector transmitted fatal visceral leishmaniasis. Commun. Biol. *4*, 929. https://doi.org/10.1038/s42003-021-02446-x.
12. Volpedo, G., Pacheco-Fernandez, T., Holcomb, E.A., Zhang, W.W., Lypaczewski, P., Cox, B., Fultz, R., Mishan, C., Verma, C., Huston, R.H., et al. (2022). Centrin-deficient Leishmania mexicana confers protection against New World cutaneous leishmaniasis.

NPJ Vaccines *7*, 32. https://doi.org/10.1038/s41541-022-00449-1.

13. Contreras, I., Estrada, J.A., Guak, H., Martel, C., Borjian, A., Ralph, B., Shio, M.T., Fournier, S., Krawczyk, C.M., and Olivier, M. (2014). Impact of Leishmania mexicana infection on dendritic cell signaling and functions. PLoS Negl. Trop. Dis. *8*, e3202. https://doi.org/10.1371/journal.pntd.0003202.
14. Cameron, P., McGachy, A., Anderson, M., Paul, A., Coombs, G.H., Mottram, J.C., Alexander, J., and Plevin, R. (2004). Inhibition of lipopolysaccharide-induced macrophage IL-12 production by Leishmania mexicana amastigotes: the role of cysteine peptidases and the NF-kappaB signaling pathway. J. Immunol. *173*, 3297–3304. https://doi.org/10.4049/jimmunol.173.5.3297.
15. Lezama-Dávila, C.M., Isaac-Márquez, A.P., Barbi, J., Oghumu, S., and Satoskar, A.R. (2007). 17Beta-estradiol increases Leishmania mexicana killing in macrophages from DBA/2 mice by enhancing production of nitric oxide but not pro-inflammatory cytokines. Am. J. Trop. Med. Hyg. *76*, 1125–1127.
16. Shweash, M., Adrienne McGachy, H., Schroeder, J., Neamatallah, T., Bryant, C.E., Millington, O., Mottram, J.C., Alexander, J., and Plevin, R. (2011). Leishmania mexicana promastigotes inhibit macrophage IL-12 production via TLR-4 dependent COX-2, iNOS and arginase-1 expression. Mol. Immunol. *48*, 1800–1808. https://doi.org/10.1016/j.molimm.2011.05.013.
17. Wilkins-Rodríguez, A.A., Escalona-Montaño, A.R., Aguirre-García, M., Becker, I., and Gutiérrez-Kobeh, L. (2010). Regulation of the expression of nitric oxide synthase by Leishmania mexicana amastigotes in murine dendritic cells. Exp. Parasitol. *126*, 426–434. https://doi.org/10.1016/j.exppara.2010.07.014.
18. Hsu, A.C., and Scott, P. (2007). Leishmania mexicana infection induces impaired lymph node expansion and Th1 cell differentiation despite normal T cell proliferation. J. Immunol. *179*, 8200–8207. https://doi.org/10.4049/jimmunol.179.12.8200.
19. Wilkins-Rodríguez, A.A., Pérez-Torres, A., Escalona-Montaño, A.R., and Gutiérrez-Kobeh, L. (2020). Differential Regulation of l-Arginine Metabolism through Arginase 1 during Infection with Leishmania mexicana Isolates Obtained from Patients with Localized and Diffuse Cutaneous Leishmaniasis. Infect. Immun. *88*, e00963-19. https://doi.org/10.1128/IAI.00963-19.
20. Volpedo, G., Pacheco-Fernandez, T., Bhattacharya, P., Oljuskin, T., Dey, R., Gannavaram, S., Satoskar, A.R., and Nakhasi, H.L. (2021). Determinants of Innate Immunity in Visceral Leishmaniasis and Their Implication in Vaccine Development. Front. Immunol. *12*, 748325. https://doi.org/10.3389/fimmu.2021.748325.
21. Saunders, E.C., and McConville, M.J. (2020). Immunometabolism of Leishmania granulomas. Immunol. Cell Biol. *98*, 832–844. https://doi.org/10.1111/imcb.12394.
22. Baardman, J., Verberk, S.G.S., Prange, K.H.M., van Weeghel, M., van der Velden, S., Ryan, D.G., Wüst, R.C.I., Neele, A.E., Speijer, D., Denis, S.W., et al. (2018). A Defective Pentose Phosphate Pathway Reduces Inflammatory Macrophage Responses during Hypercholesterolemia. Cell Rep. *25*, 2044–2052.e5. https://doi.org/10.1016/j.celrep.2018.10.092.
23. Koo, S.J., Szczesny, B., Wan, X., Putluri, N., and Garg, N.J. (2018). Pentose Phosphate Shunt Modulates Reactive Oxygen Species and Nitric Oxide Production Controlling. Front. Immunol. *9*, 202. https://doi.org/10.3389/fimmu.2018.00202.
24. Nagy, C., and Haschemi, A. (2015). Time and Demand are Two Critical Dimensions of Immunometabolism: The Process of Macrophage Activation and the Pentose Phosphate Pathway. Front. Immunol. *6*, 164. https://doi.org/10.3389/fimmu.2015.00164.
25. Moorlag, S.J.C.F.M., Rodriguez-Rosales, Y.A., Gillard, J., Fanucchi, S., Theunissen, K., Novakovic, B., de Bont, C.M., Negishi, Y., Fok, E.T., Kalafati, L., et al. (2020). BCG Vaccination Induces Long-Term Functional Reprogramming of Human Neutrophils. Cell Rep. *33*, 108387. https://doi.org/10.1016/j.celrep.2020.108387.
26. Guerrini, V., Bruiners, N., and Gennaro, M.L. (2018). Chapter 10: mTORC1 Links Cellular Metabolism and Immune Functions in *Mycobacterium tuberculosis* Infection and BCG Vaccination, Second Edition Edition (Elsevier).
27. Goll, J.B., Li, S., Edwards, J.L., Bosinger, S.E., Jensen, T.L., Wang, Y., Hooper, W.F., Gelber, C.E., Sanders, K.L., Anderson, E.J., et al. (2020). Transcriptomic and Metabolic Responses to a Live-Attenuated. Vaccines (Basel) *8*, 412. https://doi.org/10.3390/vaccines8030412.
28. Díaz, C., Pérez Del Palacio, J., Valero-Guillén, P.L., Mena García, P., Pérez, I., Vicente, F., Martín, C., Genilloud, O., Sánchez Pozo, A., and Gonzalo-Asensio, J. (2019). Comparative Metabolomics between Mycobacterium tuberculosis and the MTBVAC Vaccine Candidate. ACS Infect. Dis. *5*, 1317–1326. https://doi.org/10.1021/acsinfecdis.9b00008.
29. Liu, Y., Xu, R., Gu, H., Zhang, E., Qu, J., Cao, W., Huang, X., Yan, H., He, J., and Cai, Z. (2021). Metabolic reprogramming in macrophage responses. Biomark. Res. *9*, 1. https://doi.org/10.1186/s40364-020-00251-y.
30. Karnovsky, A., Weymouth, T., Hull, T., Tarcea, V.G., Scardoni, G., Laudanna, C., Sartor, M.A., Stringer, K.A., Jagadish, H.V., Burant, C., et al. (2012). Metscape 2 bioinformatics tool for the analysis and visualization of metabolomics and gene expression data. Bioinformatics *28*, 373–380. https://doi.org/10.1093/bioinformatics/btr661.
31. Galván-Peña, S., and O'Neill, L.A.J. (2014). Metabolic reprograming in macrophage polarization. Front. Immunol. *5*, 420. https://doi.org/10.3389/fimmu.2014.00420.
32. Bronte, V., and Zanovello, P. (2005). Regulation of immune responses by L-arginine metabolism. Nat. Rev. Immunol. *5*, 641–654.
33. Martínez-López, M., Soto, M., Iborra, S., and Sancho, D. (2018). Hijacks Myeloid Cells for Immune Escape. Front. Microbiol. *9*, 883. https://doi.org/10.3389/fmicb.2018.00883.
34. Almugadam, S.H., Trentini, A., Maritati, M., Contini, C., Rugna, G., Bellini, T., Manfrinato, M.C., Dallocchio, F., and Hanau, S. (2018). Influence of 6-aminonicotinamide (6AN) on Leishmania promastigotes evaluated by metabolomics: Beyond the pentose phosphate pathway. Chem. Biol. Interact. *294*, 167–177. https://doi.org/10.1016/j.cbi.2018.08.014.
35. Schwartz, A.G., and Pashko, L.L. (2004). Dehydroepiandrosterone, glucose-6-phosphate dehydrogenase, and longevity. Ageing Res. Rev. *3*, 171–187. https://doi.org/10.1016/j.arr.2003.05.001.
36. Rodriguez-Sosa, M., Monteforte, G.M., and Satoskar, A.R. (2001). Susceptibility to Leishmania mexicana infection is due to the inability to produce IL-12 rather than lack of IL-12 responsiveness. Immunol. Cell Biol. *79*, 320–322. https://doi.org/10.1046/j.1440-1711.2001.01014.x.
37. Weinheber, N., Wolfram, M., Harbecke, D., and Aebischer, T. (1998). Phagocytosis of Leishmania mexicana amastigotes by macrophages leads to a sustained suppression of IL-12 production. Eur. J. Immunol. *28*, 2467–2477. https://doi.org/10.1002/(SICI)1521-4141(199808)28:08<2467::AID-IMMU2467>3.0.CO;2-1.
38. Ashkani-Esfahani, S., Zarifi, F., Asgari, Q., Samadnejad, A.Z., Rafiee, S., and Noorafshan, A. (2014). Taurine improves the wound healing process in cutaneous leishmaniasis in mice model, based on stereological parameters. Adv. Biomed. Res. *3*, 204. https://doi.org/10.4103/2277-9175.142314.
39. Saini, S., and Rai, A.K. (2021). Linoleic Acid-A Feasible Preventive Approach for Visceral Leishmaniasis. Front. Nutr. *8*, 649025. https://doi.org/10.3389/fnut.2021.649025.
40. Sheedy, F.J. (2015). Turning 21: Induction of miR-21 as a Key Switch in the Inflammatory Response. Front. Immunol. *6*, 19. https://doi.org/10.3389/fimmu.2015.00019.
41. Gannavaram, S., Bhattacharya, P., Siddiqui, A., Ismail, N., Madhavan, S., and Nakhasi, H.L. (2019). miR-21 Expression Determines the Early Vaccine Immunity Induced by. Front. Immunol. *10*, 2273. https://doi.org/10.3389/fimmu.2019.02273.
42. Selvapandiyan, A., Dey, R., Nylen, S., Duncan, R., Sacks, D., and Nakhasi, H.L. (2009). Intracellular replication-deficient Leishmania donovani induces long lasting protective immunity against visceral leishmaniasis. J. Immunol. *183*, 1813–1820. https://doi.org/10.4049/jimmunol.0900276.
43. Singh, R.K., Gannavaram, S., Ismail, N., Kaul, A., Gedda, M.R., and Nakhasi, H.L. (2018). Centrin-Deleted Leishmania donovani Parasites Help CD4 + T Cells to Acquire Th1 Phenotype and Multi-Functionality Through Downregulation of CD200-CD200R Immune Inhibitory Axis. Front. Immunol. *9*, 1176. https://doi.org/10.3389/fimmu.2018.01176.
44. Karmakar, S., Volpedo, G., Zhang, W.W., Lypaczewski, P., Ismail, N., Oliveira, F., Oristian, J., Meneses, C., Gannavaram, S., Kamhawi, S., et al. (2022). Centrin-deficient Leishmania mexicana confers protection against Old World visceral leishmaniasis. NPJ Vaccines *7*, 157. https://doi.org/10.1038/s41541-022-00574-x.
45. Tomiotto-Pellissier, F., Bortoleti, B.T.d.S., Assolini, J.P., Gonçalves, M.D., Carloto, A.C.M., Miranda-Sapla, M.M., Conchon-Costa, I., Bordignon, J., and Pavanelli, W.R. (2018). Macrophage Polarization in Leishmaniasis: Broadening Horizons. Front. Immunol. *9*, 2529. https://doi.org/10.3389/fimmu.2018.02529.
46. Bogdan, C. (2020). Macrophages as host, effector and immunoregulatory cells in leishmaniasis: Impact of tissue micro-environment and metabolism. Cytokine X *2*, 100041. https://doi.org/10.1016/j.cytox.2020.100041.
47. Tannahill, G.M., Curtis, A.M., Adamik, J., Palsson-McDermott, E.M., McGettrick, A.F., Goel, G., Frezza, C., Bernard, N.J., Kelly, B.,

Foley, N.H., et al. (2013). Succinate is an inflammatory signal that induces IL-1beta through HIF-1alpha. Nature *496*, 238–242. https://doi.org/10.1038/nature11986.

48. Song, J., Sun, H., Zhang, S., and Shan, C. (2022). The Multiple Roles of Glucose-6-Phosphate Dehydrogenase in Tumorigenesis and Cancer Chemoresistance. Life *12*, 271. https://doi.org/10.3390/life12020271.
49. Frolova, A.I., O'Neill, K., and Moley, K.H. (2011). Dehydroepiandrosterone inhibits glucose flux through the pentose phosphate pathway in human and mouse endometrial stromal cells, preventing decidualization and implantation. Mol. Endocrinol. *25*, 1444–1455. https://doi.org/10.1210/me.2011-0026.
50. Daneshmandi, S., Cassel, T., Higashi, R.M., Fan, T.W.M., and Seth, P. (2021). 6-Phosphogluconate dehydrogenase (6PGD), a key checkpoint in reprogramming of regulatory T cells metabolism and function. Elife *10*, e67476. https://doi.org/10.7554/eLife.67476.
51. Bhattacharya, P., Dey, R., Dagur, P.K., Kruhlak, M., Ismail, N., Debrabant, A., Joshi, A.B., Akue, A., Kukuruga, M., Takeda, K., et al. (2015). Genetically Modified Live Attenuated Leishmania donovani Parasites Induce Innate Immunity through Classical Activation of Macrophages That Direct the Th1 Response in Mice. Infect. Immun. *83*, 3800–3815. https://doi.org/10.1128/IAI.00184-15.
52. Azevedo, E.P., Rochael, N.C., Guimarães-Costa, A.B., de Souza-Vieira, T.S., Ganilho, J., Saraiva, E.M., Palhano, F.L., and Foguel, D. (2015). A Metabolic Shift toward Pentose Phosphate Pathway Is Necessary for Amyloid Fibril- and Phorbol 12-Myristate 13-Acetate-induced Neutrophil Extracellular Trap (NET) Formation. J. Biol. Chem. *290*, 22174–22183. https://doi.org/10.1074/jbc.M115.640094.
53. Frauwirth, K.A., and Thompson, C.B. (2004). Regulation of T lymphocyte metabolism. J. Immunol. *172*, 4661–4665. https://doi.org/10.4049/jimmunol.172.8.4661.
54. Gerriets, V.A., and Rathmell, J.C. (2012). Metabolic pathways in T cell fate and function. Trends Immunol. *33*, 168–173. https://doi.org/10.1016/j.it.2012.01.010.
55. Marcinkiewicz, J., and Kontny, E. (2014). Taurine and inflammatory diseases. Amino Acids *46*, 7–20. https://doi.org/10.1007/s00726-012-1361-4.
56. Li, J., Ding, H., Meng, Y., Li, G., Fu, Q., Guo, Q., Yin, Z., Ye, Z., Zhou, H., and Shen, N. (2020). Taurine Metabolism Aggravates the Progression of Lupus by Promoting the Function of Plasmacytoid Dendritic Cells. Arthritis Rheumatol. *72*, 2106–2117. https://doi.org/10.1002/art.41419.
57. Beattie, L., Phillips, R., Brown, N., Owens, B.M.J., Chauhan, N., Dalton, J.E., and Kaye, P.M. (2011). Interferon regulatory factor 7 contributes to the control of Leishmania donovani in the mouse liver. Infect. Immun. *79*, 1057–1066. https://doi.org/10.1128/IAI.00633-10.
58. Phillips, R., Svensson, M., Aziz, N., Maroof, A., Brown, N., Beattie, L., Signoret, N., and Kaye, P.M. (2010). Innate killing of Leishmania donovani by macrophages of the splenic marginal zone requires IRF-7. PLoS Pathog. *6*, e1000813. https://doi.org/10.1371/journal.ppat.1000813.
59. Oljuskin, T., Azodi, N., Volpedo, G., Bhattacharya, P., Ismail, N., Hamano, S., Matlashewski, G., Satoskar, A.R., Gannavaram, S., and Nakhasi, H.L. (2022). *Leishmania major centrin* knock-out parasites alter the kynurenine- aryl hydrocarbon receptor signaling to produce a pro-inflammatory response. Preprint at bioRxiv. https://doi.org/10.1101/2022.09.15.508117.
60. The University of Manchester, and MIB Biospec Group Laboratory Guide for Metabolomic Experiments. www.biospec.net/wordpress/wp-content/uploads/Metabolomics-laboratory-handbook.pdf.
61. Chong, J., Soufan, O., Li, C., Caraus, I., Li, S., Bourque, G., Wishart, D.S., and Xia, J. (2018). MetaboAnalyst 4.0: towards more transparent and integrative metabolomics analysis. Nucleic Acids Res. *46*, W486–W494. https://doi.org/10.1093/nar/gky310.
62. Kanehisa, M., Goto, S., Kawashima, S., and Nakaya, A. (2002). The KEGG databases at GenomeNet. Nucleic Acids Res. *30*, 42–46. https://doi.org/10.1093/nar/30.1.42.

STAR★METHODS

KEY RESOURCES TABLE

REAGENT or RESOURCE	SOURCE	IDENTIFIER
Antibodies		
Purified anti-mouse IL-12 (p70), clone C18.2	Biolegend	Cat.No. 511802, RRID: AB_2123769
Purified anti-mouse / rat IL-1β, clone B122	Biolegend	Cat.No. 503502, RRID: AB_315287
Biotin anti-mouse IL-12/IL-23 p40, clone C17.8	Biolegend	Cat.No. 505302, RRID: AB_315374
Biotin anti-mouse IL-1β, clone Poly5158	Biolegend	Cat.No. 515801, RRID: AB_2124615
Chemicals, peptides, and recombinant proteins		
Liberase-TL	Roche	Cat.No. 5401020001
6-aminonicotinamide (6-AN)	Sigma-Aldrich	Cat.No. A68203-1G
dehydroepiandrosterone (DHEA)	Sigma-Aldrich	Cat.No. D-063
Critical commercial assays		
Griess Reagent Kit, for nitrite quantitation	Invitrogen™	G7921
Experimental models: Organisms/strains		
Leishmania mexicana Cen-/-	Volpedo et al.[12]	LmxM.22.1410
Leishmania mexicana WT	N/A	MNYC/B2/62/m379
Software and algorithms		
MetaboAnalyst 4.0.	Chong et al.[61]	https://www.metaboanalyst.ca/home.xhtml
Metscape	Karnovsky et al.[30]	http://metscape.ncibi.org/
Kyoto Encyclopedia of Genes and Genomes (KEGG)	Kanehisa et al.[62]	https://www.genome.jp/kegg/
Graph Pad Prism 9	Dotmatics	https://www.graphpad.com/

RESOURCE AVAILABILITY

Lead contact

Further information and requests for resources and reagents should be directed to and will be fulfilled by the Lead Contact and Corresponding Author, Dr. Abhay R. Satoskar (Abhay.Satoskar@osumc.edu).

Materials availability

This study did not generate new unique reagents.

Data and code availability

- All relevant data is available in the main text and supplemental information. Any additional information can be provided upon reasonable request to the authors.
- This paper does not report original code
- Any additional information required to reanalyze the data reported in this paper is available from the lead contact upon request.

EXPERIMENTAL MODEL AND SUBJECT DETAILS

Mice

Female mice with a C57BL/6 background were purchased from Envigo (Harlan laboratories) Indianapolis, IN, USA, and housed at The Ohio State University animal facility, following approved animal protocols and University Laboratory Animal Resources (ULAR) regulations (2010A0048-R3 Protocol). All the experiments were performed using 3 to 5 age-matched 5-8 week old female mice per group, randomly assigned to experimental groups (5 mice per cage). We used 3 experimental groups: 1) Naïve: non-infected mice serving as controls; 2) *LmWT:* mice infected with *L. mexicana;* and 3) *LmCen-/-:* mice infected with *L. mexicana Cen*$^{-/-}$ mutant parasites.

Parasites

LmexCen-/- have been previously generated by our group[12] by the deletion of the centrin gene (LmxM.22.1410) using CRISPR technology. *LmexCen*$^{-/-}$ and L. *mexicana* WT (MNYC/B2/62/m379) parasites were maintained via subcutaneous inoculation into the shaved back rumps of 129S6/SvEvTac mice (purchased from Taconic Biosciences, Inc.). For both parasites, amastigotes extracted from the draining lymph nodes of 129S6/SvEvTac mice were then cultured in complete M199 medium (Gibco, Thermo Fisher Scientific, Waltham, MA), complemented with 1% Penicillin/Streptomycin, 1% HEPES, and 10% fetal bovine serum (FBS) at 26°C to generate stationary phase promastigotes.

BMDMs primary culture

Bone marrow-derived macrophages (BMDMs) were isolated from the femur and tibias of C57BL/6 mice by flushing 5 ml of PBS through the bones. Then, ACK lysis buffer was used to remove red blood cells and then rinsed with ice cold PBS. After isolation, the bone marrow cell suspension was cultured with RPMI medium supplemented with 10% fetal bovine serum (FBS), 1% penicillin/streptomycin, 1% HEPES, and 20% supernatant from L-929 cells at 37°C with 5% CO_2 for 7-10 days until differentiation was complete.

METHOD DETAILS

In vivo infection

Aged-matched C57BL/6 mice were inoculated intradermally in the ear with 1×10^6 *L. mexicana* promastigotes in the stationary phase. After 7 days, the ipsilateral infected ear and the naïve ears were collected and processed for mass spectrometry.

Parasite burden determination

After 7 days of infection, the infected ears and the draining lymph nodes (dLN) were dissected and processed to obtain single cell suspensions. Briefly, dLN were disaggregated using a 70 μm strainer, whereas infected ears were digested with liberase-TL (Roche Diagnostics, 0.2mg/ml, 90 minutes at 37°C in 5% CO_2 incubator) followed by tissue disruption in a Medicon device (BD Biosciences). Then, the single cell suspensions were plated in 96 well plates in 1:10 serial dilutions using complete M199. Parasites were allowed to grow for 14 days, and the maximum dilution (log titer) where the parasites were observed (limiting dilution method) was reported.

Mass spectrometry

The ear tissue was collected, snap frozen, and processed for mass spectrometry analysis according to SOP 7 of the Laboratory Guide for Metabolomics Experiments.[60] Samples were then incubated with 500 ul of 100% MeOH and sonicated. The tissue was weighed and homogenized at 40 mg/mL of 50% MeOH solution for 3 cycles in a homogenizer with Precellys. The supernatant was collected, dried down, and reconstituted in ½ of the original volume in 5% MeOH with 0.1% formic acid.

Untargeted analysis was performed on a Thermo Orbitrap LTQ XL with HPLC separation on a Poroshell 120 SB-C18 (2x100 mm, 2.7μm particle size) with an WPS 3000 LC system. The gradient consisted of solvent A, H_2O with 0.1% Formic acid, and solvent B 100% acetonitrile at a 200μL/min flow rate with an initial 2% solvent B with a linear ramp to 95% B at 15 min, holding at 95% B for 1 minutes, and back to 2% B from 16 min and equilibration of 2% B until min 32. For each sample, 5μL were injected and the top 5 ions were selected for data dependent analysis with a 15 second exclusion window.

For feature selection in the untargeted results analysis, including database comparison and statistical processing, samples were analyzed in Progenesis QI and the pooled sample runs were selected for feature alignment. Anova p-value scores between the groups were calculated with a cutoff of < 0.05. With database matching using the [Human Metabolome Database], selecting for adducts M+H, M+Na, M+K, and M+2H and less than 10ppm mass error, unique features were tentatively identified as potential metabolites.

Pathway analysis of MS datasets

We have used two different techniques in order to identify enriched pathways in our data sets. First, we used the Functional Analysis Module (MS peaks to pathways) in MetaboAnalyst 4.0.[61] Detected peaks (mass-to-charge ratios + retention times) from positive and negative analytical modes of the mass spectrometer for each sample were organized into four column lists along with calculated p-values and t-scores from univariate t-tests. These peak list profiles were uploaded to the functional analysis module and passed the internal data integrity checks. The ion mode in MetaboAnalyst was set to the appropriate type depending on the analytical mode that was used to generate the data. For each analysis the mass tolerance was set to 10 ppm, the retention time units were set to minutes, and the option to enforce primary ions was checked. In parameter settings, the mummichog algorithm (version 2.0) and the modified gene set enrichment algorithm were used for all analyses. The p-value cutoff for the mummichog algorithm was left at the default (top 10% of peaks). Currency metabolites and adducts were left at default settings. Lastly, the Kyoto Encyclopedia of Genes and Genomes (KEGG)[62] pathway library for *Mus musculus* was selected as the metabolic network that the functional analysis module would use to infer pathway activity and predict metabolite identity; only pathways/metabolite sets with at least three entries were allowed.

In vitro cell culture and infection

Differentiated BMDMs were plated in a 24-well plate at a density of $0.5x10^6$ per well and infected overnight with stationary phase *LmexCen*$^{-/-}$ promastigotes at a ratio of 10:1 (parasite to macrophages). The naïve controls were treated with media alone. Then, the extracellular parasites were removed by washing with PBS and new media was applied. Some of the groups were stimulated with LPS (0.75μg/ml) for 24 hrs after infection and then washed with PBS. Some of the groups were then treated with 100μM 6-aminonicotinamide (6-AN) or dehydroepiandrosterone (DHEA) (both from Sigma-Aldrich), two pentose phosphate pathway inhibitors.[22] After a 24hrs incubation, the supernatant was collected to measure nitric oxide and cytokine levels.

Nitric oxide assay

Nitric oxide release from BMDMs was determined in the culture supernatants by measurement of nitrite using Griess Reagent Kit (Invitrogen) and sodium nitrite as the standard. A Molecular Devices SpectraMax M3 microplate reader was used to measure the absorbance at 570 nm, and concentrations of nitric oxide were determined from the standard curve with the Softmax Pro software (Molecular Devices LLC).

Cytokine ELISA

Levels of IL-12 and IL-1β in BMDM supernatants were determined by sandwich ELISA. 96-well plates were coated with primary capture antibody against IL-12 and IL-1β at a final concentration of 2μg/ml, and incubated overnight at 4°C. Plates were then blocked with PBS + 10% FBS for 2 hrs at RT and incubated overnight with 50 μl of culture supernatants or recombinant cytokine (standard curve) in duplicates at 4°C. After washing with PBS-Tween (0.05% Tween 20 in 1× PBS, pH 7.4), the plates were incubated with biotinylated detection antibodies against IL-12 and IL-1β at a final concentration of 1μg/ml, for 1 hr at RT, washed again, and incubated with streptavidin-conjugated Alkaline Phosphatase for 30 mins at RT in the dark. After washing again, the plates were incubated with PNPP until development. A Molecular Devices SpectraMax M3 microplate reader was used to measure absorbance at 405 nm, and the SoftMax Pro software was used to quantify cytokine levels against the standard curve. All reagents for ELISA were purchased from Biolegend Inc.

QUANTIFICATION AND STATISTICAL ANALYSIS

All *in vitro* and *in vivo* data show a representative experiment with $N \geq 3$ per group. N represents different biological replicates. For the nitric oxide assay, unpaired two-tailed Mann-Whitney t test was performed using Graph Pad Prism 9 to compare statistical significance. A p value < 0.05 was considered significant. In all figures * represents $p \leq 0.05$, ** represents $p \leq 0.01$ and *** represents $P \leq 0.001$ (also found in the figure legends). Error bars represent SEM (standard error of the mean).

Statistical analysis of MS datasets

For the mass spectrometry data all statistical analysis were performed with MetaboAnalyst software. Peak intensity data tables from the mass spectrometry experiment were formatted into comma-separated values (CSV) files conforming to MetaboAnalyst's requirements and uploaded into the one-factor statistical analysis module. Each analysis passed MetaboAnalyst's internal data integrity check and additional data filtering was performed based on interquartile range. On the normalization overview page, sample normalization was performed based on the median of the data and the auto-scaling option was chosen to perform data scaling; No transformation of the data was performed. For dimensionality reduction, both principal component analysis (PCA) and partial least-squares discriminant analysis (PLS-DA) were employed. Cross-validated sum of squares (Q2) performance measures were used to determine if PLS-DA models were overfitted. Visualization of significant, differentially regulated metabolites was done by generating volcano plots with cutoffs of <0.05 false-discovery rate (FDR) and >2-fold change (FC). Clustering of samples and features were analyzed by creating dendrograms and hierarchical heatmaps, respectively.